Express Polymer Letters Vol.17, No.5 (2023) 502–511
Available online at www.expresspolymlett.com
https://doi.org/10.3144/expresspolymlett.2023.37

Research article

Copper-coated hollow glass microspheres filled rubber composites: Lightweight, interface bonding and mechanical properties

Leyuan Ma, Yiming Wang, Xin Zhang, Shibao Wen, Zhen Yu, Zhenxiu Zhang*

Key Laboratory of Rubber–Plastics, Ministry of Education/Shandong Provincial Key Laboratory of Rubber–Plastics, Qingdao University of Science and Technology, 266042 Qingdao, China

Received 16 September 2022; accepted in revised form 9 December 2022

Abstract. In this work, cis-1,4-polybutadiene rubber/polystyrene-butadiene rubber (BR/SBR) blend was filled with inorganic lightweight filler hollow glass microspheres (HGMs) to develop a rubber-based lightweight composite. Cu-plating was carried out on the surface of HGMs by polydopamine (PDA) and Ag nanoparticles to improve the compatibility among HGMs and rubber matrix. Filter paper experiment, X-ray energy dispersive spectroscopy (EDS) and X-ray photoelectron spectrometer (XPS) were used to analyze the bonding mechanism between Cu-plated HGMs and rubber. The results confirmed that the redox reaction between the reactive sulfur in the rubber matrix and Cu on the surface of Cu-plated HGM can be successfully carried out at 170 °C. And the compatibility between HGM and rubber matrix was obviously improved after Cu plating. The physical-mechanical properties and abrasion resistance of the composites were improved significantly. This research was of great significance to marine flexible floating body materials.

Keywords: *polymer composites, rubber, coatings, mechanical properties, lightweight*

1. Introduction

Polymer-based lightweight materials have wide application prospects in daily life, ocean engineering, space exploration, and other fields [1–4]. Reducing the density of the polymer while maintaining the mechanical properties is beneficial to reduce the cost and improve the operation efficiency [5, 6]. Hollow glass microspheres (HGMs) are vitreous hollow spheres with a particle size of micron level and a density of 0.12~0.60 g·cm^{-3}. Synthetic HGMs have the advantages of stable physical properties, less stress concentration, and controllable density. Doping in the polymer matrix not only improves the modulus and strength of the composite material but also has obvious weight reduction, sound insulation, and thermal insulation effects. At present, HGMs are often used in the preparation of marine floating materials. Generally, HGMs is doped in an epoxy resin (EP) matrix and prepared by an epoxy resin curing process [4, 7, 8], which is a hard, brittle, and low-density composite material.

Surface modification of HGMs is usually required to improve properties of doped HGMs composites, such as silane coupling agents [9–11] and surface metallization modification [12, 13]. Li *et al*. [14] demonstrated that silane coupling agents enhanced the adhesion between the HGMs and epoxy resin matrix, resulting in enhanced compressive and tensile performance compared to those prepared using unmodified HGMs. Nam *et al*. [15] modified the surface of HGMs with silane coupling agents to improve the compatibility with the rubber matrix, which improved the mechanical properties of the composite material.

---

*Corresponding author, e-mail: zhangzhenxiu@qust.edu.cn

Lee *et al*. [16] reported that a multifunctional biopolymer thin-coating polydopamine (PDA) layer can be formed on a variety of inorganic and organic materials by self-polymerization of dopamine in an aqueous solution. The self-polymerization of dopamine provides an easy one-step surface functionalization method with simple composition, mild reaction conditions, and applicability to various types of materials [17, 18]. More importantly, the PDA layer can be used as a general platform for secondary reactions [19]. The noble metal ion-binding ability of catechol present in the PDA structure has been specifically exploited to deposit uniform, continuous and dense metal coatings on various substrates by electroless plating, which is no need for traditional cumbersome and environmentally unfriendly activation and sensitization processes [20, 21].

In the tire industry, the steel cord of an all-steel radial tire usually needs to be copper-plated to improve its adhesion to the rubber [22, 23]. It can be seen that copper plating on the surface of the material is a method to improve its adhesion to rubber. However, how to improve the bonding with polymer and the properties of the composite by Cu plating HGMs is still a problem to be solved.

In this study, cis-1,4-polybutadiene rubber/polystyrene-butadiene rubber (BR/SBR) blend was used as the substrate to carry out lightweight composite by filling modified HGMs. We used a novel PDA modified HGMs-nano silver particle catalytic Cu plating process, which was inspired by the Cu plating of steel cords in industrial automotive all-steel radial tires. The binding mechanism of Cu-plated HGMs and rubber matrix was studied, and the physical and mechanical properties of the composites were analyzed.

2. Experimental materials and methods

2.1. Experimental materials

BR (BR9000) and SBR (SBR1502) were purchased from Sinopec (Yanshan, China). Carbon black (CB, N550) was purchased from Black Cat Carbon Black Co. LTD (Jingdezhen, China). HGMs (HGS8000X) with an average density of 0.42 $g\cdot cm^{-3}$ and compressive pressure of 55.1 MPa was purchased from 3M Company (Saint Paul, USA). Dopamine hydrochloride ($DA\cdot HCl$, analytical pure (AR)), tris(hydroxymethyl)aminomethane (Tris, AR), and dimethylamine borane (DMAB, AR), dioctyl phthalate (DOP, chemically pure (CP)) were purchased from Aladdin (Shanghai, China). Silver nitrate ($AgNO_3$, AR), anhydrous copper sulfate ($CuSO_4$, AR), potassium sodium tartrate ($KNaC_4H_2O\cdot 4H_2O$, AR), hydrochloric acid (HCl, AR), anhydrous ethanol (C_2H_6O, AR) and boric acid (H_3BO_3, AR), tetramethylthiuram disulfide (TMTD, CP), sulfur (S, CP), *N*-cyclohexyl-2-benzothiazolesulfenamide (CBS, CP), *N*-cyclohexyl-2-benzothiazolesulfenamide (CZ, CP), and 1,2-dihydro-2,2,4-trimethylquinoline (RD, CP) were obtained from Sinopharm Group Chemical Co., Ltd. (Shanghai, China). Stearic acid (SA, CP), zinc oxide (ZnO, CP) and microcrystalline wax (MSW, CP) were obtained from Chemtronics Fine Chemicals Co. (Shanghai, China).

2.2. The preparation process

The process schematic is shown in Figure 1. HGMs were placed in a beaker with anhydrous ethanol and cleaned for 30 min at room temperature to remove impurities from the surface. Then, the HGMs were taken out and heated in an oven at 60 °C for 1 h to completely evaporate the absolute ethanol. 210 g HGMs and 1.0 g $DA\cdot HCl$ were put into 500 ml weakly alkaline buffer solution with pH value 8.5 and continuously stirred at 40 °C for 24 h. In this case, dopamine generated polydopamine (PDA) through its own oxidative polymerization and coated on HGMs surface. After centrifugation, the HGMs/PDA was washed and filtered with deionized water. The prepared HGMs/PDA was placed in 50 mM $AgNO_3$ solution and stirred for 1.5 h with a volume liquor ratio of 1:1. After that, the turbid liquid containing glass microbeads was washed and filtered by deionized water to obtain the surface-activated HGMs/PDA$_{Ag}$.

The Cu plating solution included 50 mmol/l $CuSO_4$ (copper plating main salt), 70 mmol/l $NaC_4H_4O_6\cdot 4H_2O$ (Cu^+ complexing agent), 0.1 mol/l DMAB (reducing agent) and 0.1 mol/l H_3BO_3 (stabilizer). The prepared HGMs/PDA$_{Ag}$ was dispersed in the

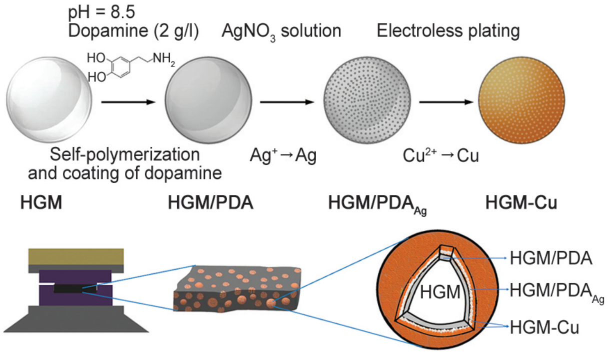

Figure 1. The composite material preparation process.

Table 1. The formula of BR/SBR.

Composition	SBR	BR	CB	S	TMTD	CZ	CBS	ZnO	DOP	MSW	RD
Content [phr]	70	30	50	1.5	0.5	1	2	5	10	2	1

plating solution at 35 °C for 1.5 h, where the volume bath ratio was 1:1.5. The cloudy solution of glass beads was filtered and washed with deionized water and dried at 40 °C for 5 h to obtain Cu-coated HGMs, which was named HGMs-Cu.

10, 20, 30, 40, and 50% volume contents of HGMs-Cu were mixed with BR/SBR, respectively, and the formula of BR/SBR is shown in Table 1. Then the composites were vulcanized at 170 °C and 10 MPa for 30 min with a plate vulcanizer to prepare sheets with a thickness of 2 and 8 mm.

2.3. Characterization

Scanning electron microscopy (SEM, JSM-7500F, JEOL, Tokyo, Japan) was used to investigate the composite structure. The sample was broken in liquid nitrogen and sputtered with a thin layer of gold in the fracture surface. The X-ray energy dispersive spectroscopy (EDS) equipped with the SEM was used to analyze the surface elements.

In order to characterize the loading of silver nanoparticles and copper plating on the surface of HGMs, X-ray diffraction analyzer (XRD, UltimaIV, Rigaku Corporation, Tokyo, Japan) was used to test the crystal morphology of HGMs samples at various stages, and the diffraction angle (2θ) ranged from 5 to 90°.

In order to verify the adhesion mechanism between HGMs-Cu and rubber, we tried to use a filter paper experiment [24], *i.e.*, place a layer of filter paper on the surface of the BR/SBR compound to isolate the HGMs-Cu from the compound so that the HGMs-Cu and the compound could not be in direct contact, and spread another layer of filter paper on the other side to sandwich the HGMs-Cu in the middle of the rubber compound, as shown in Figure 2. In this way, during the vulcanization process, reactive ions can pass through the filter paper to reach the surface of HGMs-Cu to produce a chemical reaction. After the film was cured, the vulcanized rubber on both sides of the filter paper was carefully peeled off and the HGMs-Cu samples were collected for analysis. X-ray photoelectron spectrometer (XPS, Thermo Fisher Scientific, Massachusetts, USA) was used to analyze the elemental map of the HGMs-Cu sample after the filter paper experiment to characterize the valence state of sulfur and copper on the surface of the material.

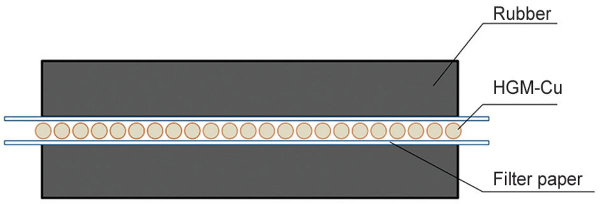

Figure 2. Brief schematic diagram of filter paper experiment.

Tensile strength tests of the composite material were performed by a servo control tensile testing machine (AI-7000S, GO TECH, Taipei, China) with a clamps speed of 200 mm·min^{-1} at 23 °C, and the specimens were 4 mm width and 2 mm thickness. The apparent density of the composite material was determined according to the ASTM D 792 method by weighing the sample in air and water using an electronic density meter (GT-XB320M, GO TECH, Taipei, China).

The abrasion resistance of the composite material samples was measured with a DIN abrasion tester (GT-7012-D, GO TECH, Taipei, China) based on the ISO 4649-2002 standard. The machine has an abrasive drum coated with abrasive paper with a particle size of P60 (423 grains). A cylindrical disc specimen with a diameter of 13 mm and a thickness of 8 mm was installed on the specimen holder and pressed against the abrasive drum under a load of 10 N. When the test starts, the abrasive drum rotates at 40 rpm and the specimen moves horizontally on the drum. The test is terminated when the specimen has completed one horizontal movement along the drum. The weight loss due to abrasion is determined from the initial and final weights of the specimens. Three specimens of each sample were subjected to the wear test. From the average weight loss obtained and the density value of the sample, the relative volume loss (ΔV_{rel}) was calculated by Equation (1):

$$\Delta V_{\mathrm{rel}} = \frac{\Delta m_{\mathrm{t}} \cdot \Delta m_{\mathrm{const}}}{\rho_{\mathrm{t}} \cdot \Delta m_{\mathrm{r}}} \qquad (1)$$

where Δm_{t} and Δm_{r} are the mass loss values of the experimental and comparison specimen, respectively, $\Delta m_{\mathrm{const}}$ is the constant mass loss value of the comparison specimen, and ρ_{t} is the density of the experimental specimen.

3. Results and discussion

3.1. Physical and chemical structure analysis of HGMs-Cu

Compared with the surface morphologies HGMs (Figure 3a), The surface of the HGMs/PDA (Figure 3b) was relatively dull and rough, which is due to the self-polymerization of dopamine in a weak alkaline environment [20], and no local defects (due to the production process) were observed, which may have been filled with polydopamine. The surface of the HGMs mainly contained O, Si, and Ca (Figure 4a), but C element could be clearly observed from the EDS spectrum of HGMs/PDA (Figure 4b). The appearance of C accounted for 24.43% of the elements, which came from the PDA macromolecular layer. No scattering peak of N element was found because N accounts for a small proportion in PDA (4%), which has been masked by other strong scattering peak signals.

The surface of HGMs/PDA$_{Ag}$ was shiny and rougher, and a layer of 'powder' was attached to the surface of the microspheres (Figure 3c). Because Ag$^+$ in silver nitrate was adsorbed by a large amount of catechol in the molecular structure of PDA. This group had a unique reducing property for noble metal ions and reduced Ag$^+$ in situ, which was finally absorbed in the form of Ag nanoparticles on the PDA surface [20]. From the EDS spectrum of HGMs/PDA$_{Ag}$ (Figure 4c), it can be seen that 1.59% Ag element after the surface Ag$^+$ activation of HGMs/PDA microspheres.

After electroless Cu plating, the surface of HGMs-Cu microbeads was rougher (Figure 3d), the coating on the surface has been evolved to 'fine sand' and the particle size was obviously increased. This was because, in the process of electroless Cu plating, the Ag particles on the surface of the HGMs/PDA$_{Ag}$ microspheres play a catalytic role, and the Cu^{x+} in the

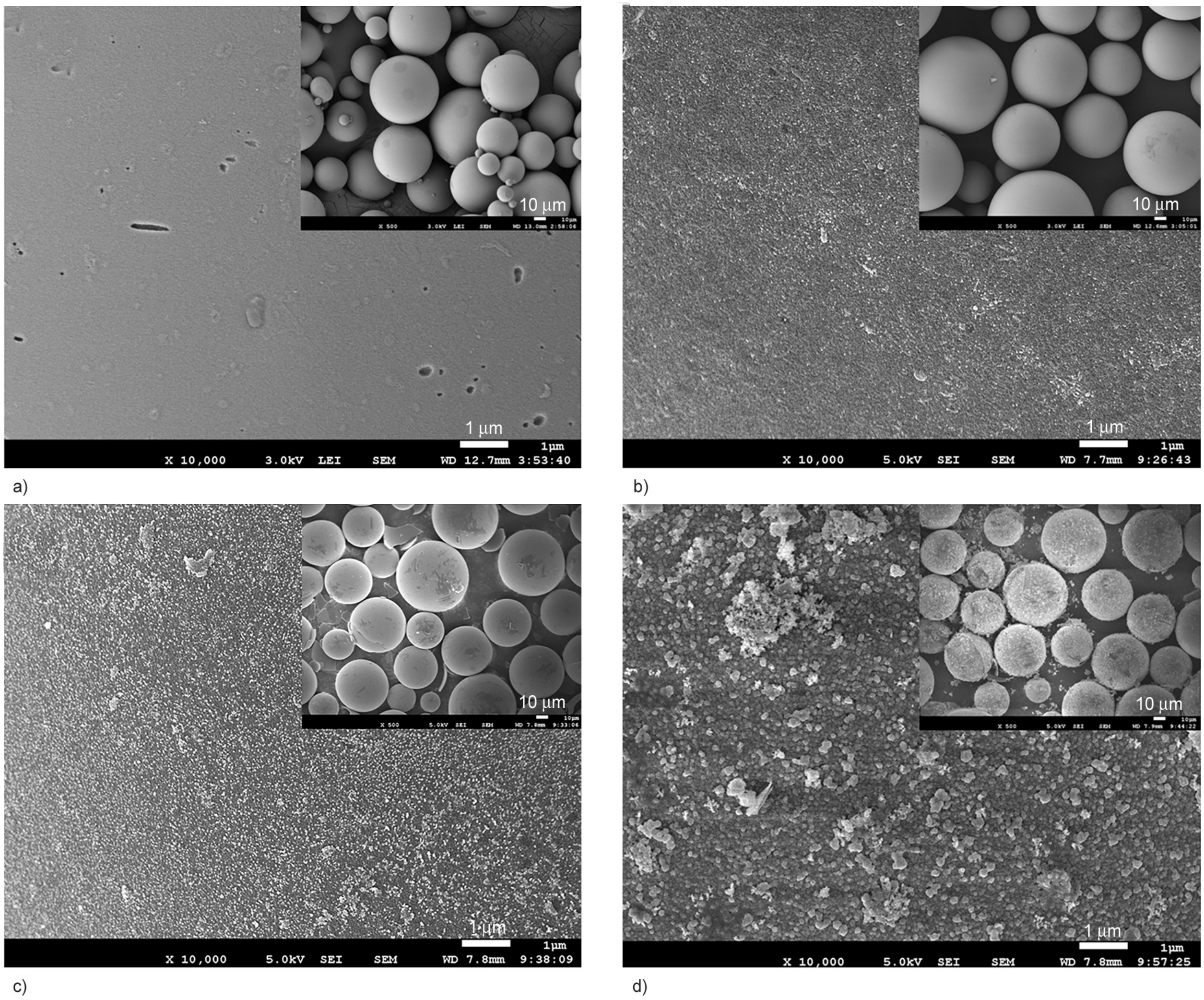

Figure 3. Surface morphology of a) HGMs, b) HGMs/PDA, c) HGMs/PDA$_{Ag}$ and d) HGMs-Cu.

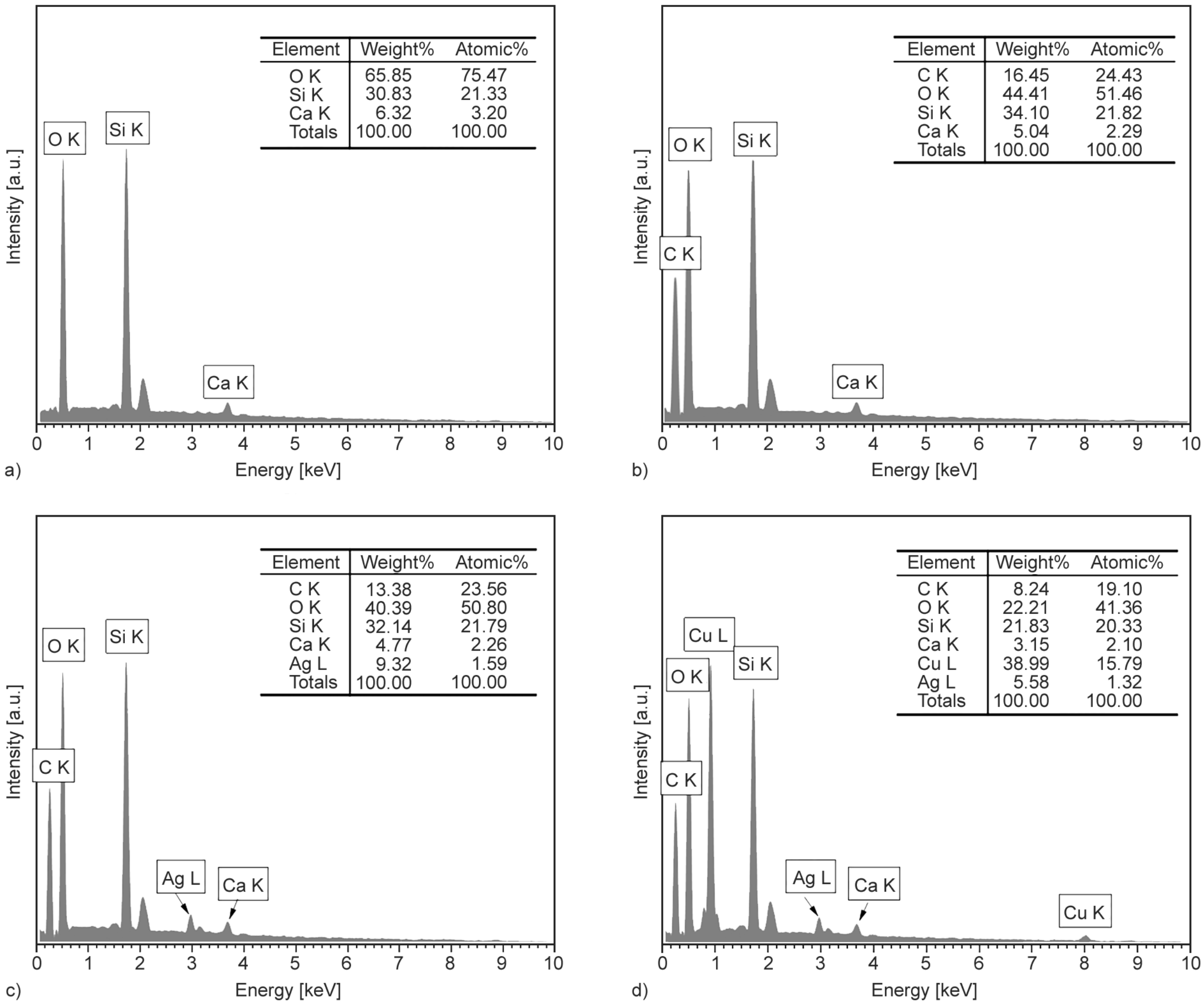

Figure 4. EDS spectra of a) HGMs, b) HGMs/PDA, c) HGMs/PDA$_{Ag}$ and d) HGMs-Cu (The peak around 2.1 KeV is Pt).

plating solution took the Ag particles as the grain nucleation center and reduced to Cu by the reducing agent DMAB. In addition, the Cu element accounted for 15.79% on the surface of the HGMs (Figure 4d). Figure 5 shows the XRD patterns of the samples at various stages of the electroless copper plating process. The HGMs had a large envelope peak at around 22°, which indicated that the HGMs exist in an amorphous state, and the spectrum of HGMs/PDA was almost no different from the HGMs [25]. It was consistent with the results of Hu *et al.* [21]. After the HGMs were activated by Ag$^+$, the characteristic peaks of low-intensity Ag particles appeared in the diffraction pattern at 38.2, 44.4, 64.5, 77.5, and 81.5°, which were consistent with the standard PDF card JCPDS. No. 4-783, corresponding to the (111), (200), (220), (311), and (322) crystal planes in the single-mass face-centered cubic crystal structure of silver [20, 21]. After electroless Cu plating, the HGMs-Cu microspheres showed strong copper characteristic peaks at 43.4, 50.6 and 74.2°, which were consistent with the standard PDF card JCPDS No. 4-836, corresponding to the three crystal planes (111), (200) and (220) in the single-mass face-centered cubic crystal structure of Cu. In addition, no other oxidation peak of Cu was found, indicating

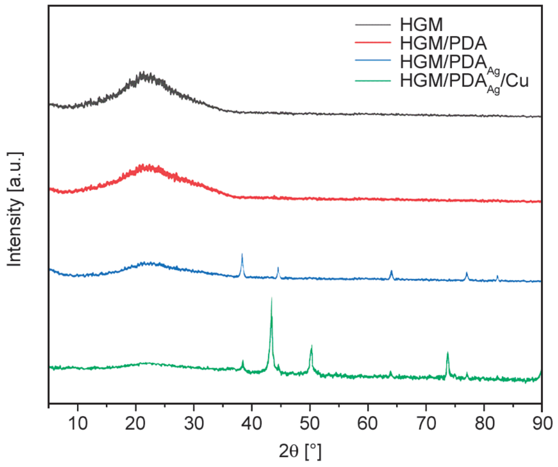

Figure 5. XRD spectra of HGMs at various stages of the electroless copper plating process.

that the material was not oxidized during the drying process of the vacuum oven.

3.2. Interface bonding between HGMs-Cu and BR/SBR

In order to verify the adhesion mechanism between copper-coated HGMs and rubber, a filter paper experiment is designed (Figure 2). The surface morphology and chemical analysis of HGMs-Cu after the filter paper experiment are shown in Figure 6. Compared with the HGMs-Cu before the filter paper experiment (Figure 4d), the sulfur (S) was newly added to the energy spectrum after the filter paper experiment (Figure 6a). It could be inferred that the S element came from the rubber matrix. The active S successfully passed through the thin filter paper, and there was a possibility of a redox reaction at high temperature with the Cu on the surface HGMs-Cu (Equation (2)):

$$2\mathrm{Cu} + \mathrm{S} \xrightarrow{\Delta} \mathrm{Cu_2S} \qquad (2)$$

In order to further verify the reaction between the Cu layer on the HGMs-Cu surface and the S in the rubber matrix, we performed an XPS test and analysis. It can be seen that the observed elements in XPS full spectrum (Figure 6b) were basically the same as the EDS energy spectrum (Figure 6a). The appearance of the N_{1s} peak at 400 eV in the XPS full spectrum is attributed to the $–NH_2$ group in the polydopamine basal layer on the bead surface.

It can be seen from Figure $6b_1$ that the peak positions of the binding energy of Cu_{2p} were located at 952.3 and 932.4 eV, which indicated that the Cu on the surface of the HGMs-Cu after the filter paper experiment may exist in the form of Cu^0 and Cu^{x+} [26]. In addition, Figure $6b_2$ shows that the peak position of the kinetic energy of Cu_{LM2} was located at 916.4 eV, which was further indicated that the Cu element on the surface existed in the form of Cu^{x+} [27, 28]. The peak position of S_{2p} was located at 162.3 eV as shown in Figure $6b_3$, indicating that the S element on the HGMs-Cu after the filter paper experiment mainly existed in the form of S^{2-} [29].

Therefore, combined with the EDS and XPS analysis results, it can be proved that there was Cu_2S on the surface of the HGMs-Cu after the filter paper experiment, indicating that the S in the rubber matrix successfully passed through the gap of the filter paper and adsorbed on HGMs-Cu surface. Furthermore, a redox reaction occurred with the Cu during the high-temperature co-vulcanization process. Therefore, the Cu and S near the bonding interface of the HGMs-Cu and the BR/SBR reacted to form a Cu_xS layer, which was embedded with the rubber phase. That was to say the adhesion of HGMs-Cu to rubber mainly depended on the tight intercalation between Cu_xS layer and rubber [24]. The combined schematic diagram is shown in Figure 7.

3.3. Physical and mechanical properties analysis

Figure 8 shows that with the increase of HGMs and HGMs-Cu, the density of the composites decreased gradually. When the added amount is 50 vol%, the density of BR/SBR/HGMs and BR/SBR/HGMs-Cu was 0.76 and 0.82 $g{\cdot}cm^{-3}$, respectively. The density of BR/SBR/HGMs-Cu was slightly higher than that of BR/SBR/HGMs, which was attributed to the coated layer on the surface of HGMs-Cu. To be specific, the average density of HGM and HGM-Cu were 0.420 and 0.455 $g{\cdot}cm^{-3}$.

The tensile strength of the composite material showed a downward trend with the increase of volume fraction, but BR/SBR/HGMs-Cu was slightly higher than BR/SBR/HGMs (Figure 9a). When the material was subjected to external tensile force, the HGMs and rubber matrix were prone to detachment, the interface of the HGMs became the stress concentration point of the external tensile force (Figure 9c). With the increase of HGMs content, the distance between HGMs per unit volume decreased, and the stress concentration effect became more obvious. Hence, the BR/SBR/HGMs tensile strength decreased significantly with the increased HGMs content. The tensile strength of BR/SBR/HGMs-Cu increased slightly to 11.4 MPa with 10 vol% HGMs-Cu, because of the better interface bonding between HGMs-Cu and the rubber matrix (Figure 9d). The bonding between the HGMs-Cu and the rubber matrix provided an interfacial relationship. The bridging effect of HGMs-Cu acted as a part of the stress concentration point when the rubber phase, which enhanced the ability of BR/SBR/HGMs-Cu to endure external stress. When the content of HGMs-Cu continued to increase, the bonding between HGMs-Cu and rubber required the participation of S in the rubber matrix to produce the rubber. The S content was constant in the rubber formulation, and the S content available for the rubber matrix for vulcanization reaction decreased with the

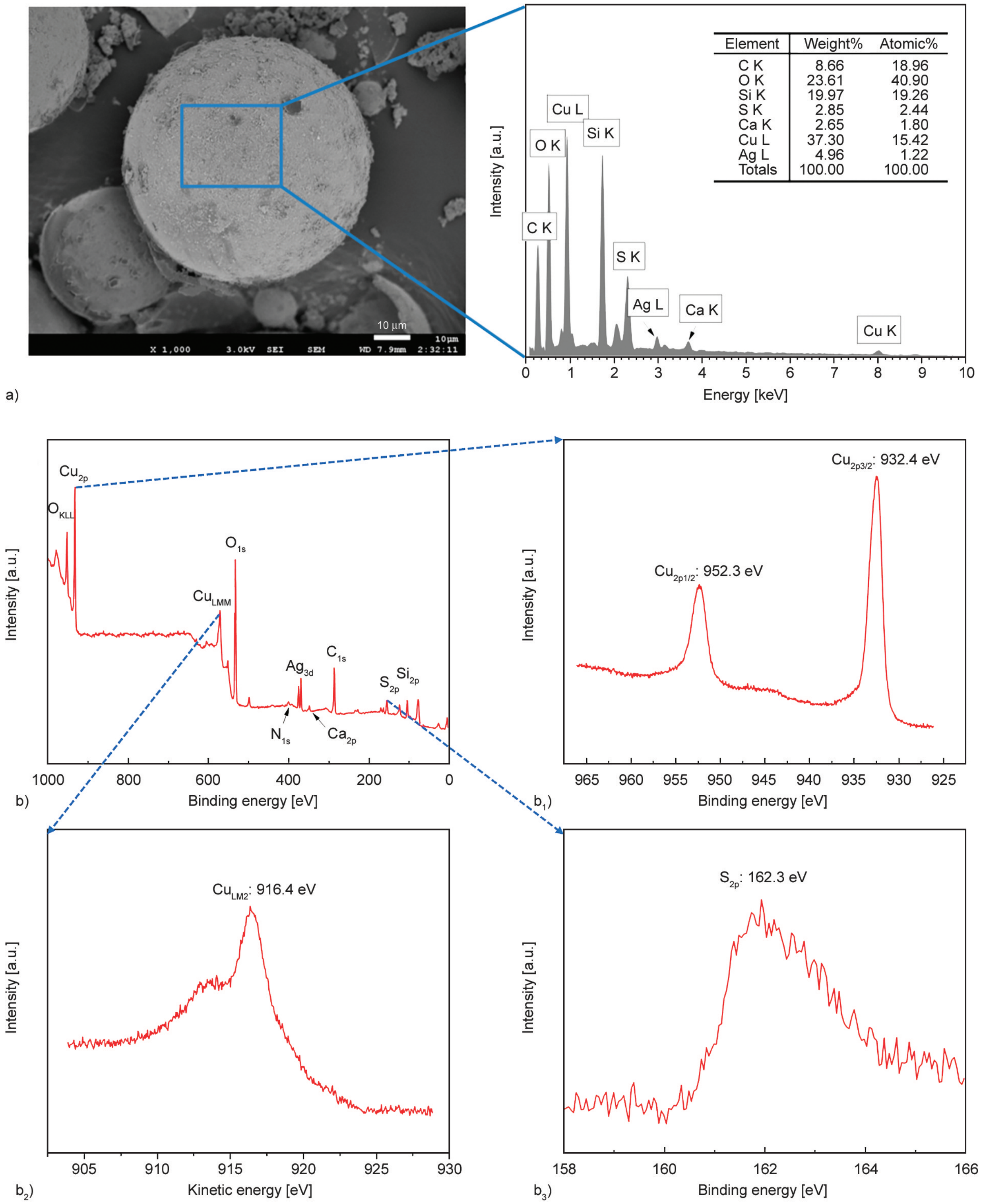

Element	Weight%	Atomic%
C K	8.66	18.96
O K	23.61	40.90
Si K	19.97	19.26
S K	2.85	2.44
Ca K	2.65	1.80
Cu L	37.30	15.42
Ag L	4.96	1.22
Totals	100.00	100.00

Figure 6. a) EDS spectrum b) XPS wide-scan spectrum of HGMs-Cu after filter paper experiment: b$_1$), b$_2$) Cu spectrum and b$_3$) S spectrum.

redox reaction between the Cu and S, which eventually led to the vulcanization decrease of the rubber matrix, resulting in reduced tensile resistance.

Figure 9b shows the effect of the content of HGMs and HGMs-Cu on the relative volume loss of the composites. The relative volume loss of BR/SBR/HGMs increased sharply with the increase of HGMs content. When the content of HGMs added in the composite material reaches 50 vol%, the relative volume loss has reached 289 mm^3. The obvious increase in the relative volume loss was due to poor bonding between the HGMs-Cu and the rubber matrix

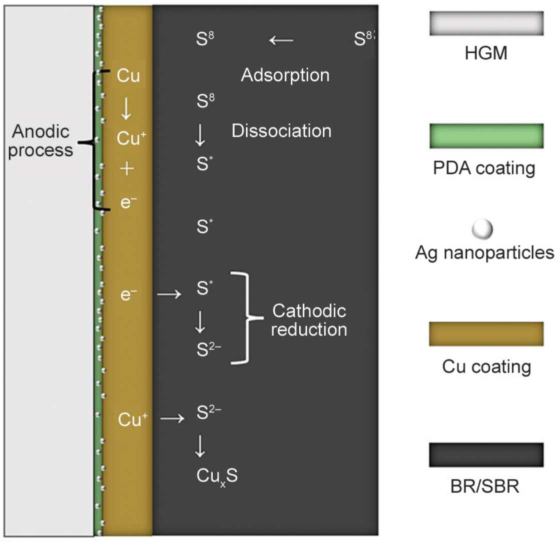

Figure 7. Schematic diagram of the chemical bonding process of HGMs-Cu and BR/SBR.

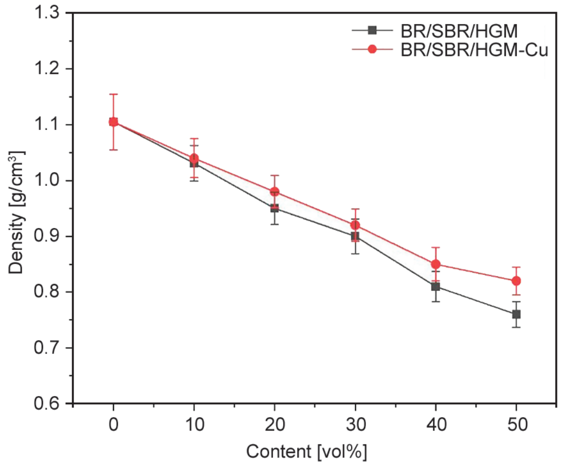

Figure 8. Influence of the content of HGMs and HGMs-Cu on the density of the composites.

(Figure 9c). The HGMs was easy to peel off from the rubber matrix, which resulted in a loss of the wear volume of the composite material. When the content of HGMs-Cu in the BR/SBR/HGMs-Cu reached 50 vol%, the relative volume loss was 187 mm^3, which was 102 mm^3 lower than that of the

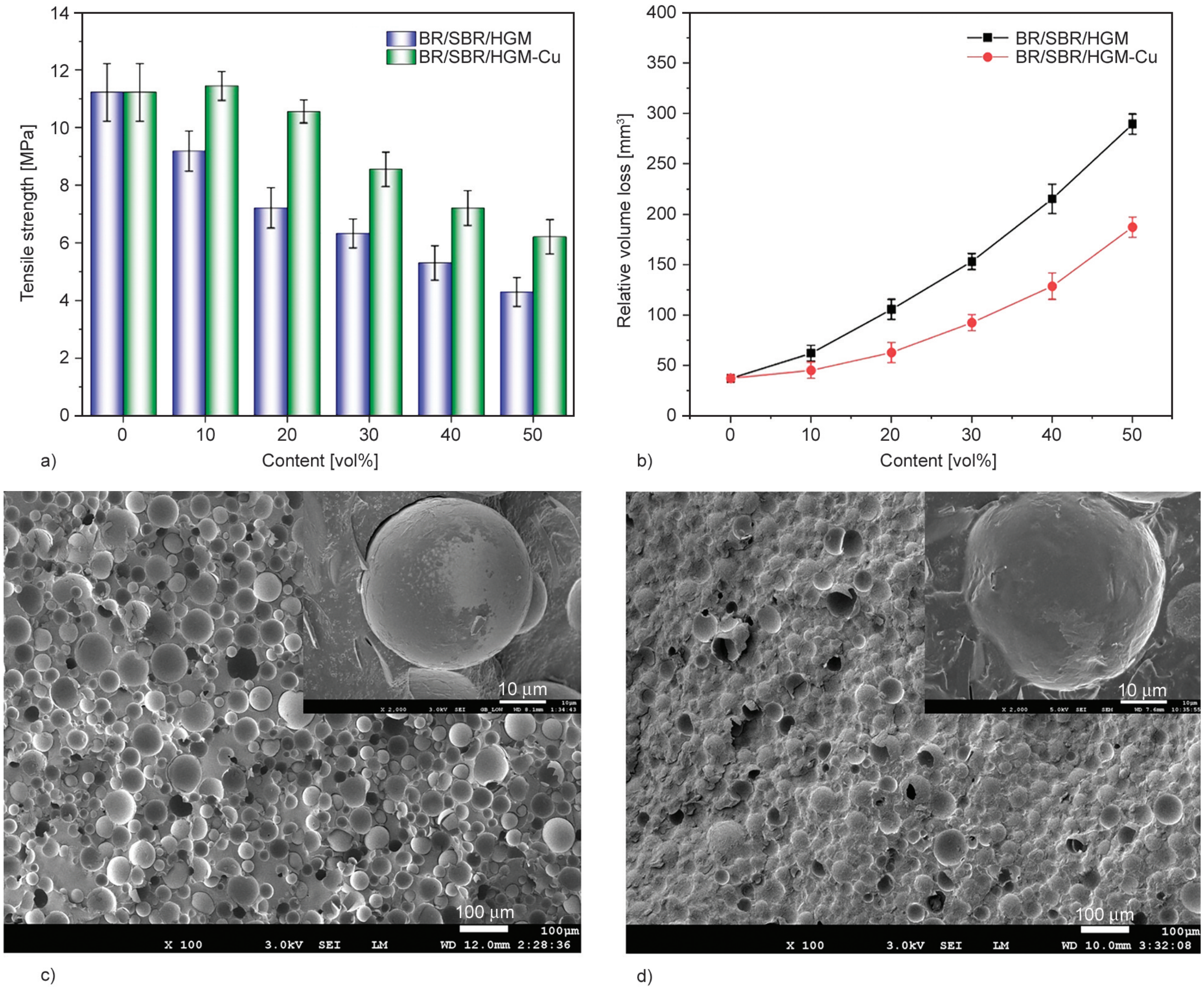

Figure 9. a) Tensile strength and b) relative volume loss of the composites with different HGMs or HGMs-Cu content; the section morphology of c) BR/SBR/HGMs and d) BR/SBR/HGMs-Cu.

BR/SBR/HGMs because there was a chemical bound between the HGMs-Cu and rubber matrix.

4. Conclusions

Herein, HGMs-Cu was prepared by Cu plating on HGMs with PDA modification and Ag^+ catalysis; then the lightweight BR/SBR/HGMs-Cu composites were prepared through co-vulcanization. The compatibility, performance, and adhesion mechanism of the HGMs-Cu and BR/SBR matrix were analyzed.

Dopamine underwent the oxidative polymerization reaction in a weak alkaline (pH = 8.5) water bath to form PDA and adhere on the HGMs surface, which provided a secondary reactive active surface. These reactive groups of PDA reduced Ag^+ in situ to Ag on the surface of the HGMs/PDA_{Ag}, which acted as the reduction and activation center of Cu^{2+} in the further electroless plating process. The XPS and EDS analysis proved that Cu_xS formed between HGMs-Cu and BR/SBR, which improved the interface combining ability. In addition, the density of the composite decreased almost linearly with the increase in HGMs content. When the addition amount of HGMs-Cu reached 50 vol%, the density was 0.82 $g \cdot cm^3$, which was larger than that of BR/SBR/HGMs (0.76 $g \cdot cm^3$) due to the coated layer. But the tensile strength of the BR/SBR/HGMs-Cu was higher than that of BR/SBR/HGMs, when the HGMs-Cu amount was 10 vol%, and the tensile strength of the BR/SBR/HGMs-Cu was 11.4 MPa. In addition, when the content of HGMs-Cu in the composite reached 50 vol%, the relative volume loss of BR/SBR/HGMs-Cu was 187 mm^3, which was 102 mm^3 lower than that oBR/SBR/HGMs. The analysis further indicated that the Cu-plated particles had a better binding ability with rubber, which can improve the properties of lightweight rubber and broaden its application.

References

[1] Wang Y., Yu Z., Phule A. D., Zhao Y., Wen S., Zhang Z. X.: A lightweight, abrasion-resistant polybutadiene rubber/styrene butadiene rubber foam prepared by three-step process for footwear outsole applications. Macromolecular Materials and Engineering, **307**, 2100702 (2022).
https://doi.org/10.1002/mame.202100702

[2] Zhang Z. X., Wang Y. M., Zhao Y., Zhang X., Phule A. D.: A new TPE-based foam material from EPDM/PPB blends, as a potential buffer energy-absorbing material. Express Polymer Letters, **15**, 89–103 (2021).
https://doi.org/10.3144/expresspolymlett.2021.10

[3] Salama A., Li L., Mativenga P., Whitehead D.: TEA CO_2 laser machining of CFRP composite. Applied Physics A- Materials Science & Progressing, **122**, 497 (2016).
https://doi.org/10.1007/s00339-016-0025-8

[4] Ding J., Liu Q., Ye F., Zhang H., Gao Y., Zhang B.: Compressive properties of *co*-continuous hollow glass microsphere/epoxy resin syntactic foams prepared using resin transfer molding. Journal of Reinforced Plastics and Composites, **39**, 132–143 (2020).
https://doi.org/10.1177/0731684419877568

[5] Blanco D., Rubio E. M., Lorente-Pedreille R., Sáenz-Nuño M. A.: Lightweight structural materials in open access: Latest trends. Materials, **14**, 6577 (2021).
https://doi.org/10.3390/ma14216577

[6] Xu J., Mkaddem A., El Mansori M.: Recent advances in drilling hybrid FRP/Ti composite: A state-of-the-art review. Composite Structures, **135**, 316–338 (2016).
https://doi.org/10.1016/j.compstruct.2015.09.028

[7] Gao G., Hu Y., Jia H., Liu P., Du P., Xu D.: Acoustic and dielectric properties of epoxy resin/hollow glass microsphere composite acoustic materials. Journal of Physics and Chemistry of Solids, **135**, 109105 (2019).
https://doi.org/10.1016/j.jpcs.2019.109105

[8] Imran M., Rahaman A., Pal S.: Effect of low concentration hollow glass microspheres on mechanical and thermomechanical properties of epoxy composites. Polymer Composites, **40**, 3493–3499 (2019).
https://doi.org/10.1002/pc.25211

[9] Zhang L., Zhang J., Wang D-Y.: Hierarchical layered double hydroxide nanosheets/phosphorus-containing organosilane functionalized hollow glass microsphere towards high performance epoxy composite: Enhanced interfacial adhesion and bottom-up charring behavior. Polymer, **210**, 123018 (2020).
https://doi.org/10.1016/j.polymer.2020.123018

[10] Huang C., Huang Z., Qin Y., Ding J., Lv X.: Mechanical and dynamic mechanical properties of epoxy syntactic foams reinforced by short carbon fiber. Polymer Composites, **37**, 1960–1970 (2016).
https://doi.org/10.1002/pc.23374

[11] Ge H., Jin X., Liu Z., Wang C., Wang P.: Compressive property and thermal stability of GO@hollow glass microsphere/epoxy resin lightweight composites. Journal of Nanoscience and Nanotechnology, **17**, 3217–3223 (2017).
https://doi.org/10.1166/jnn.2017.13045

[12] Zhang J., Yang X., Yu S., Ge M., Meng F., Wang J., Wu X., Jiang W.: Roughening of hollow glass microspheres by NaF for Ni electroless plating. Surface & Coatings Technology, **359**, 62–72 (2019).
https://doi.org/10.1016/j.surfcoat.2018.12.031

[13] Xu R., Wang W., Yu D.: Preparation of silver-plated hollow glass microspheres and its application in infrared stealth coating fabrics. Progress in Organic Coatings, **131**, 1–10 (2019).
https://doi.org/10.1016/j.porgcoat.2019.02.009

[14] Li R., Fan G., Wang P., Ouyang X., Ma N., Wei H.: Effects of silane coupling agent modifications of hollow glass microspheres on syntactic foams with epoxy matrix. Polymers & Polymer Composites, **29**, 1191–1203 (2021).
https://doi.org/10.1177/09673911211046796

[15] Nam Y. S., Yu J-K., Park G. W., Kim H. J., Kim D. G., Kim M., Hyun K.: Effect of surface modification of hollow glass microspheres (HGM) in rubber composites (in Korean). Polymer- Korea, **43**, 567–574 (2019).
https://doi.org/10.7317/pk.2019.43.4.567

[16] Lee H., Dellatore S. M., Miller W. M., Messersmith P. B.: Mussel-inspired surface chemistry for multifunctional coatings. Science, **318**, 426–430 (2007).
https://doi.org/10.1126/science.1147241

[17] Yang D., Tian M., Wang W., Li D., Li R., Liu H., Zhang L.: Controllable dielectric and electrical performance of polymer composites with novel core/shell-structured conductive particles through biomimetic method. Electrochimica Acta, **87**, 9–17 (2013).
https://doi.org/10.1016/j.electacta.2012.08.122

[18] Sharma S. Mudgal D. Gupta V.: Polydopamine coating on additive manufacturing-based poly lactic acid structures with controllable parameters for enhanced mechanical properties: An experimental investigation. Polymer Engineering and Science, **62**, 3523–3542 (2022).
https://doi.org/10.1002/pen.26124

[19] Yilmaz A., Yilmaz M.: Bimetallic core-shell nanoparticles of gold and silver *via* bioinspired polydopamine layer as surface-enhanced Raman spectroscopy (SERS) platform. Nanomaterials, **10**, 688 (2020).
https://doi.org/10.3390/nano10040688

[20] Lee H. A., Ma Y. F., Zhou F., Hong S., Lee H.: Material-independent surface chemistry beyond polydopamine coating. Accounts of Chemical Research, **52**, 704–713 (2019).
https://doi.org/10.1021/acs.accounts.8b00583

[21] Hu J., Wu S., Cao Q., Zhang W.: Synthesis of core-shell structured alumina/Cu microspheres using activation by silver nanoparticles deposited on polydopamine-coated surfaces. RSC advances, **6**, 81767–81773 (2016).
https://doi.org/10.1039/C6RA09106G

[22] Kannan M. P., Som A., Ahuja T., Subramanian V., Nair A. S., Pradeep T.: Nonstoichiometric copper sulfide nanostructures at the brass-rubber interface: Implications for rubber vulcanization temperature in the tire industry. ACS Applied Nano Materials, **3**, 7685–7694 (2020).
https://doi.org/10.1021/acsanm.0c01298

[23] Paulthangam K. M., Som A., Ahuja T., Srikrishnarka P. Nair A. S., Pradeep T.: Role of zinc oxide in the compounding formulation on the growth of nonstoichiometric copper sulfide nanostructures at the brass-rubber interface. ACS Omega, **7**, 9573–9581 (2022)
https://doi.org/10.1021/acsomega.1c06207

[24] van Ooij W. J.: Mechanism of rubber-to-brass adhesion: Effect of rubber composition on the adhesion. Rubber Chemistry and Technology, **51**, 52–71 (1978).
https://doi.org/10.5254/1.3535727

[25] Fu Y., Liu L., Zhang L., Wang W.: Highly conductive one-dimensional nanofibers: Silvered electrospun silica nanofibers via poly(dopamine) functionalization. ACS Applied Materials & Interfaces, **6**, 5105–5112 (2014).
https://doi.org/10.1021/am5002663

[26] Dolma P., Banotra A., Padha N., Khosla A.: Sequentially evaporated layer deposition stack of CuxS thin films for photonics applications. Journal of Materials Research and Technology, **20**, 3760–3771 (2022).
https://doi.org/10.1016/j.jmrt.2022.08.097

[27] Zhang X., Guo Y., Zhang P., Wu Z., Zhang Z.: Superhydrophobic CuO@Cu_2S nanoplate vertical arrays on copper surfaces. Materials Letters, **64**, 1200–1203 (2010).
https://doi.org/10.1016/j.matlet.2010.02.050

[28] Briggs D.: Handbook of X-ray photoelectron spectroscopy CD wanger. Physical Electronics Division, Eden Prairie, (1981).

[29] Dong G., Wang Y., Jiang W. J., Zou Y., Ma Z.: Interface adhesion properties characterization of sulfide electrode materials by the combination of BOLS and XPS. Science China-Technology Sciences, **65**, 1798–1807 (2022).
https://doi.org/10.1007/s11431-022-2054-4